PHYSICAL REVIEW B **92**, 161109(R) (2015)

Optical properties of the perfectly compensated semimetal WTe_2

C. C. Homes,[1,*] M. N. Ali,[2] and R. J. Cava[2]

[1]*Condensed Matter Physics and Materials Science Department, Brookhaven National Laboratory, Upton, New York 11973, USA*

[2]*Department of Chemistry, Princeton University, Princeton, New Jersey 08544, USA*

(Received 8 June 2015; revised manuscript received 11 August 2015; published 12 October 2015)

The optical properties of layered tungsten ditelluride have been measured over a wide temperature and frequency range for light polarized in the *a*-*b* planes. A striking low-frequency plasma edge develops in the reflectance at low temperature where this material is a perfectly compensated semimetal. The optical conductivity is described using a two-Drude model which treats the electron and hole pockets as separate electronic subsystems. At low temperature, one scattering rate collapses by over two orders of magnitude, while the other also undergoes a significant, but less dramatic, decrease; both scattering rates appear to display the quadratic temperature dependence expected for a Fermi liquid. First principles electronic structure calculations reveal that the low-lying optical excitations are due to direct transitions between the bands associated with the electron and hole pockets.

DOI: 10.1103/PhysRevB.92.161109 PACS number(s): 78.30.−j, 71.20.Be, 72.15.Lh, 78.20.−e

Materials containing tellurium display a wide range of electronic properties that make them of interest for a variety of different applications, including photovoltaics [1], thermoelectrics [2], *p*-type semiconductors [3], topological insulators [4], and superconductors [5]. To add to this wide variety of phenomena, it has recently been proposed that the layered transition metal dichalcogenide WTe_2 is a perfectly compensated semimetal at low temperature [6], i.e., the number of electrons and holes per unit volume is identical. A simple two-band model predicts that the magnetoresistance will saturate at high fields, unless the material is compensated, in which case the magnetoresistance will increase quadratically with field [7]. The magnetoresistance of WTe_2 increases in precisely such a fashion; moreover, it becomes extremely large at low temperature and shows no signs of saturation, even at very high fields [6]. Electronic structure and transport studies indicate that there are electron and hole pockets in this material [8,9], and angle resolved photoemission studies show that at low temperature they are almost exactly the same size [10,11], resulting in a perfectly compensated semimetal. The zero-field behavior is equally dramatic, with a very large residual resistivity ratio of $\rho(300\ \mathrm{K})/\rho(5\ \mathrm{K}) \simeq 300$, with $\rho(5\ \mathrm{K}) \simeq 2 \times 10^{-6}\ \Omega\,\mathrm{cm}$ [6]. It is expected that such a dramatic change in the resistivity should produce striking changes in the optical properties of this material.

In this Rapid Communication the optical properties of WTe_2 are determined in the *a*-*b* plane in the absence of a magnetic field over a wide frequency and temperature range. The reflectance reveals the formation of a striking low-frequency plasma edge at low temperature. The complex conductivity indicates that the electron and hole pockets give rise to carriers with dramatically different scattering rates. While both follow a quadratic temperature dependence and may be thought of as Fermi liquids, one scattering rate decreases by more than two orders of magnitude at low temperature and is responsible for the formation of a plasma edge in the reflectance. Previous electronic structure calculations are reproduced, showing electron and hole pockets of roughly equal size, and extended to include the real part of the in-plane optical conductivity. The low-energy interband transitions are shown to originate from direct transitions between the bands associated with the hole and electron pockets.

Single crystals of WTe_2 were grown using a bromine vapor transport method [6]. WTe_2 crystallizes in the orthorhombic $Pmn2_1$ space group [12], where the tungsten atoms form chains along the *a* axis and lie between sheets of tellurium atoms, forming the *a*-*b* planes. The sheets stack along the *c* axis and are easily exfoliated (inset of Fig. 1). The foil-like platelets were glued to a metal backing plate for support and then mounted on optically black cones. The temperature dependence of the reflectance, shown in Fig. 1, was measured for light polarized in the *a*-*b* planes over a wide frequency range ($\simeq$2 meV to 3 eV) using an *in situ* overcoating technique [13]. The low-frequency reflectance is characteristic of a metallic response, increasing dramatically with decreasing temperature and revealing a sharp plasma edge at $\sim$300–400 cm^{-1}. The optical conductivity has been determined from a Kramers-Kronig analysis of the reflectance [14], which requires that the reflectance be supplied over the entire frequency range; below the lowest measured frequency a metallic Hagen-Rubens form has been employed, $1 - R(\omega) \propto \sqrt{\omega}$, while above the highest measured frequency the reflectance is assumed to decrease as $1/\omega$ up to 1.5×10^5 cm^{-1}, above which a free-electron $1/\omega^4$ extrapolation was used [15].

The optical conductivity in the infrared region is shown in Fig. 2. At high temperatures the response may be reasonably described by a single Drude component (a Lorentzian centered at zero frequency where the full width at half maximum is the free-carrier scattering rate) that gives way to a midinfrared response that is dominated by interband transitions. As the temperature is reduced, this Drude-like feature narrows considerably, leading to a transfer of spectral weight (area under the conductivity curve) from high to low frequency, revealing several interband transitions, shown more clearly in the inset of Fig. 2. Above 2000 cm^{-1} (0.25 eV) the optical conductivity increases linearly with frequency until roughly 1 eV; we argue that this linear behavior is due to the superposition of several different interband transitions and not due to a strong renormalization of the free-carrier scattering rate [16,17]. At high temperatures there is reasonable agreement with

*homes@bnl.gov

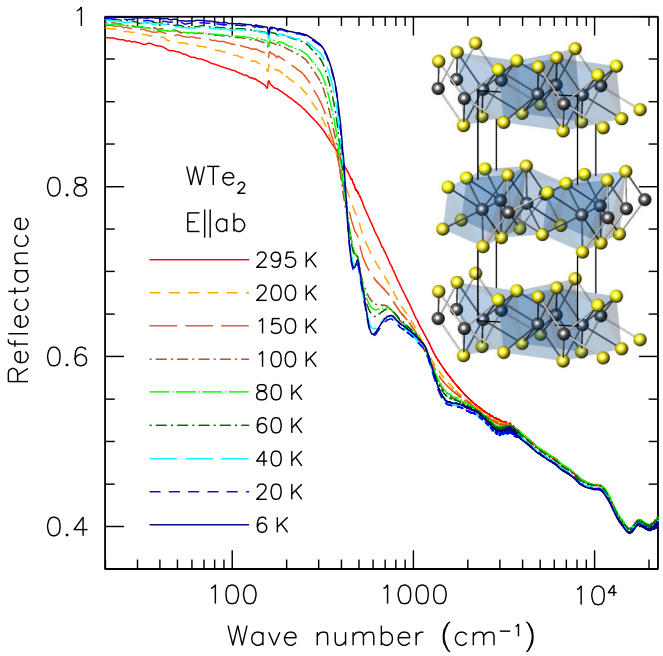

FIG. 1. (Color online) The temperature dependence of the reflectance in the infrared region of WTe_2 for light polarized in the *a*-*b* planes, revealing the formation of a sharp plasma edge in the reflectance with decreasing temperature. Inset: The unit cell is shown for the *b*-*c* face projected along the *a* axis.

$\sigma_1(\omega \to 0)$ and the transport values for $\sigma_{DC} = 1/\rho$. However, at low temperatures a single Drude component is not capable of describing both the extremely high values for σ_{DC} and the shape of the low-frequency conductivity. Given that there are both electron and hole pockets in this material, it is appropriate to employ a model that accounts for both types of carriers [18]. The complex dielectric function $\tilde{\epsilon} = \epsilon_1 + i\epsilon_2$ of the so-called two-Drude model is

$$\tilde{\epsilon}(\omega) = \epsilon_\infty - \sum_{j=1}^{2} \frac{\omega_{p,j}^2}{\omega^2 + i\omega/\tau_j} + \sum_k \frac{\Omega_k^2}{\omega_k^2 - \omega^2 - i\omega\gamma_k}, \quad (1)$$

where ϵ_∞ is the real part at high frequency. In the first sum $\omega_{p,j}^2 = 4\pi n_j e^2/m_j^*$ and $1/\tau_j$ are the square of the plasma frequency and scattering rate for the delocalized (Drude) carriers in the jth band, respectively, and n_j and m_j^* are the carrier concentration and effective mass. In the second summation, ω_k, γ_k, and Ω_k are the position, width, and strength of the kth vibration or bound excitation. The complex conductivity is $\tilde{\sigma}(\omega) = \sigma_1 + i\sigma_2 = -2\pi i\,\omega[\tilde{\epsilon}(\omega) - \epsilon_\infty]/Z_0$, where $Z_0 \simeq 377\ \Omega$ is the impedance of free space, yielding units for the conductivity of $\Omega^{-1}\,\mathrm{cm}^{-1}$.

The two-Drude model is fit simultaneously to both σ_1 and σ_2 using a nonlinear least-squares method. The fit to the data at 100 K shown in Fig. 3 indicates that the optical conductivity can be reproduced quite well using two Drude components, in addition to a series of Lorentzian oscillators at $\simeq$800, 1100 and 1950 cm^{-1} ($\simeq$100, 136 and 240 meV); other bound excitations above $\simeq$3500 cm^{-1} (430 meV) are also included in the total fit but not discussed. At 100 K the two Drude contributions

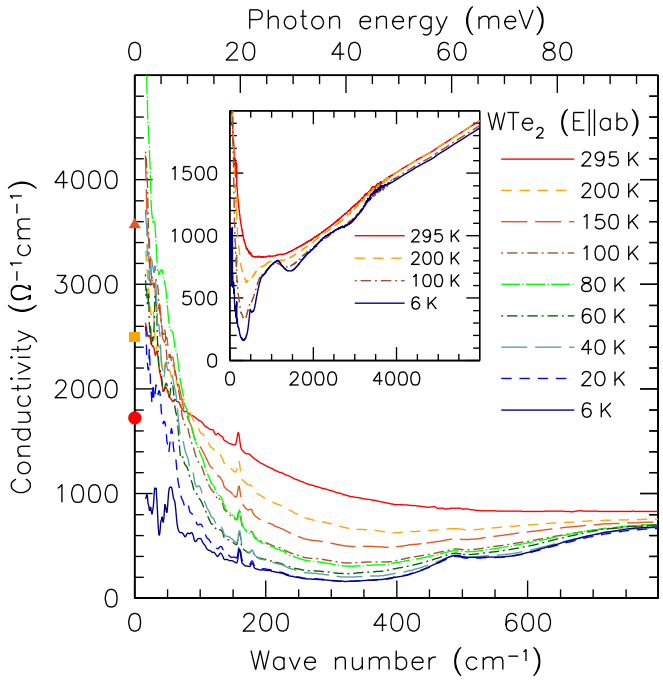

FIG. 2. (Color online) The temperature dependence of the real part of the optical conductivity of WTe_2 for light polarized in the *a*-*b* planes. The symbols along the *y* axis denote the values for σ_{DC} obtained from transport measurements [6]. Inset: The optical conductivity for a restricted set of temperatures over a wider frequency range.

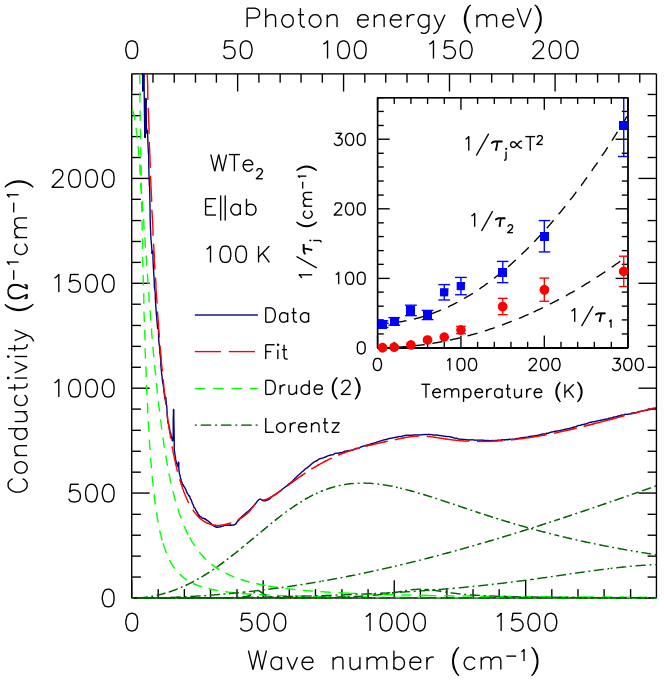

FIG. 3. (Color online) The fit to the complex optical conductivity of WTe_2 at 100 K. The fit is composed of two Drude responses (dashed lines) and several Lorentzian features (dotted-dashed lines); the linear combination (long-dash line) reproduces the real part of the optical conductivity quite well. Inset: The fitted values for $1/\tau_1$ (circles) and $1/\tau_2$ (squares); the dashed lines are drawn as a guide to the eye.

TABLE I. Transport values ρ and σ_0, and optical scattering rates $1/\tau_1$ and $1/\tau_2$.

T (K)	ρ[a] ($\mu\Omega$ cm)	σ_0 ($\times 10^3$ Ω^{-1} cm^{-1})	$1/\tau_1$ (cm^{-1})	$1/\tau_2$ (cm^{-1})
295	580	2.07	110 ± 22	320 ± 45
200	400	3.00	84 ± 16	160 ± 22
150	280	4.28	60 ± 12	109 ± 15
100	150	8.00	26 ± 5	89 ± 12
80	100	12.0	16 ± 3	80 ± 11
60	70	17.2	12 ± 2	47 ± 6
40	30	40.0	4.1 ± 0.8	54 ± 7
20	7	171	0.90 ± 0.2	38 ± 5
6	2	600	0.25 ± 0.05	34 ± 4

[a]Reference [6].

are of roughly equal weight with $\omega_{p,1} = 3000 \pm 200$ cm^{-1}, $1/\tau_1 = 26 \pm 5$ cm^{-1} and $\omega_{p,2} = 3400 \pm 200$ cm^{-1}, $1/\tau_2 = 89 \pm 12$ cm^{-1}; fits at 80 and 150 K returned similar values for the plasma frequencies, so they have been assumed to be temperature independent and are not fitted parameters. While fitting to both scattering rates at 100 K works reasonably well, at higher temperatures the broad nature of the conductivity leads to larger values for the scattering rates and increasing uncertainties. At lower temperatures the dramatic increase in σ_{DC} below 100 K suggests that $1/\tau_1$ is becoming too small to be reliably determined from fits to $\tilde{\sigma}(\omega)$. In order to provide an anchor for the fits to the scattering rates, $1/\tau_1$ is first estimated from the Drude formula $1/\tau_1 = 2\pi\,\omega_{p,1}^2/(Z_0\sigma_0)$. For those temperatures where a direct comparison between transport and optics is possible, it appears that $\sigma_0 = \sigma_1(\omega \to 0) \simeq 1.2\sigma_{DC}$, so we have used the approximation $\sigma_0 \simeq 1.2\sigma_{DC}$. Treating $1/\tau_1$ as static, only $1/\tau_2$ is fit to the optical conductivity, allowing the contribution $\sigma_{02} = 2\pi\,\omega_{p,2}^2\,\tau_2/Z_0$ to be calculated where $\sigma_0 = \sigma_{01} + \sigma_{02}$; the iterative improvement in $1/\tau_1$ is determined from $1/\tau_1 = 2\pi\,\omega_{p,1}^2/(Z_0\sigma_{01})$. The temperature dependence of the transport values of ρ, σ_0, and the scattering rates determined in this fashion are summarized in Table I. The temperature dependence of $1/\tau_1$ and $1/\tau_2$ is shown in the inset of Fig. 3 as circles and squares, respectively. While there is some uncertainty of the scattering rates at high temperature, in both cases they follow a roughly quadratic temperature dependence, suggesting both sets of carriers resemble a Fermi liquid [19–21]. While $1/\tau_2$ decreases by roughly an order of magnitude at low temperature, it does not rival the dramatic collapse of $1/\tau_1$ from $\simeq$110 cm^{-1} at 295 K to $\simeq$0.3 cm^{-1} at 5 K, associated with the formation of the plasma edge in the reflectance. At low temperature the extremely large, nonsaturating magnetoresistance indicates that this material is perfectly compensated [10], i.e., $n_1 = n_2$. From the values of $\omega_{p,1}$ and $\omega_{p,2}$, it may be shown that carrier masses are similar, $m_2 \simeq 0.8m_1$, in good agreement with Shubnikov–de Haas oscillation measurements [22].

There are a series of excitations in the infrared at $\simeq$100, 136, and 240 meV, as well as several others above 0.4 eV; these absorptions are in general quite broad and have a substantial amount of spectral weight at low frequency. Previous band structure studies of WTe_2 revealed a semimetallic character with small electron and hole pockets [6,9]; these results have been reproduced and extended in this work (the details of the calculations [23–25] are discussed in the Supplemental Material [26]).

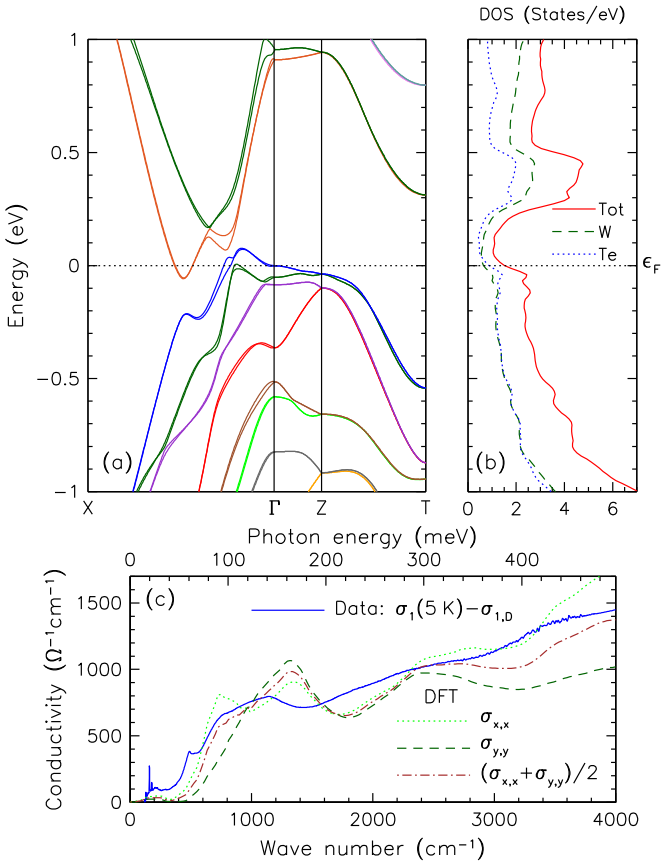

FIG. 4. (Color online) (a) The calculated electronic structure of WTe_2 including the effects of spin-orbit coupling between several different high-symmetry points of the orthorhombic Brillouin zone. (b) The total density of states (DOS), including the contributions from the W and Te atoms. (c) The real part of the calculated optical conductivity $\sigma_{x,x}$,$\sigma_{y,y}$ and the average of the two, compared to the measured optical conductivity at 5 K with the Drude terms removed.

The calculated electronic band structure including the effects of spin-orbit coupling is shown in Fig. 4(a) for paths between several different high-symmetry points in the orthorhombic Brillouin zone, revealing both electron and hole bands in the Γ-X direction, in good agreement with previous results [6,9]. A more detailed examination of the band structure (see the Supplemental Material) reveals several bands that lie just above and below the Fermi level ϵ_F that may be responsible for the low-energy interband transitions. To explore this further, the total density of states (DOS) for the W and Te atoms is calculated using a fine k-point mesh (10 000 k points) and shown in Fig. 4(b). The low value for the DOS at ϵ_F is consistent with the semimetallic nature of this material. The prominent increase in the DOS in the 200–500 meV above ϵ_F is larger than 50–150 meV interval over which interband transitions are observed in the optical conductivity. However, the optical conductivity is a reflection of the joint density of states (JDOS) rather than just the DOS. The real part of the optical conductivity has been

calculated [27] using the same fine k-point mesh for $\sigma_{x,x}$ and $\sigma_{y,y}$ (a and b axes, respectively), shown in Fig. 4(c), and is compared to the experimental value for the conductivity at 5 K with the Drude contributions removed. Both $\sigma_{x,x}$ and $\sigma_{y,y}$ have a very weak absorption at about 25 meV with the onset of much stronger absorptions occurring above about 50 meV, with $\sigma_{x,x}$ displaying prominent features at $\simeq$80 and 160 meV, while only the 160 meV peak is present in $\sigma_{y,y}$; above $\simeq$200 meV the two conductivities continue to increase steadily with frequency. The average of the two curves reproduces the experimental data reasonably well. The details of the contributions to the optical conductivity (see the Supplemental Material) reveal that these two strong absorptions at 80 and 160 meV originate from direct transitions between the bands associated with the hole and electron pockets. The feature at 60 meV, which occurs at too high an energy to be a lattice vibration [28], remains unexplained; however, it has been shown that there are very low-energy excitations in this material. Because this feature only emerges at low temperature where the material is perfectly compensated, it is likely that it is due to a low-energy interband transition that is sensitive upon the details of the band structure that may not captured in this calculation.

To conclude, the complex optical properties of the perfectly compensated semimetal WTe_2 have been measured in the a-b planes for a variety of temperatures over a wide frequency range. The electron and hole pockets are described using the two-Drude model, revealing that as the temperature is reduced, one scattering rate collapses by over two orders of magnitude, resulting in the formation of a striking plasma edge in the reflectance, while the other scattering rate is considerably larger and does not decrease by nearly the same amount. Both sets of carriers may be described as Fermi liquids. The calculated optical conductivity indicates that low-energy absorptions are due to direct transitions between the bands associated with the hole and electron pockets. The emergence of a narrow low-energy absorption at low temperature is thought to be a low-lying interband transition related to subtle changes in the electronic structure that result in a perfectly compensated semimetal.

We would like to acknowledge illuminating discussions with T. Valla. This work is supported by the Office of Science, U.S. Department of Energy under Contract No. DE-SC0012704 and by the Army Research Office, Grant No. W911NF-12-1-0461.

[1] B. M. Basol and B. McCandless, J. Photonics Energy **4**, 040996 (2014).
[2] H. J. Goldsmid, Materials **7**, 2577 (2015).
[3] K. E. Petersen, U. Birkholz, and D. Adler, Phys. Rev. B **8**, 1453 (1973).
[4] X.-L. Qi and S.-C. Zhang, Rev. Mod. Phys. **83**, 1057 (2011).
[5] T. J. Liu, J. Hu, B. Qian, D. Fobes, Z. Q. Mao, W. Bao, M. Reehuis, S. A. J. Kimber, K. Prokeš, S. Matas, D. N. Argyriou, A. Hiess, A. Rotaru, H. Pham, L. Spinu, Y. Qiu, V. Thampy, A. T. Savici, J. A. Rodriguez, and C. Broholm, Nat. Mater. **9**, 718 (2010).
[6] M. N. Ali, J. Xiong, S. Flynn, J. Tao, Q. D. Gibson, L. M. Schoop, T. Liang, N. Haldolaarachchige, M. Hirschberger, N. P. Ong, and R. J. Cava, Nature (London) **514**, 205 (2014).
[7] E. Fawcett and W. A. Reed, Phys. Rev. **131**, 2463 (1963).
[8] S. Kabashima, J. Phys. Soc. Jpn. **21**, 945 (1966).
[9] J. Augustin, V. Eyert, T. Böker, W. Frentrup, H. Dwelk, C. Janowitz, and R. Manzke, Phys. Rev. B **62**, 10812 (2000).
[10] I. Pletikosić, M. N. Ali, A. V. Fedorov, R. J. Cava, and T. Valla, Phys. Rev. Lett. **113**, 216601 (2014).
[11] J. Jiang, F. Tang, X. C. Pan, H. M. Liu, X. H. Niu, Y. X. Wang, D. F. Xu, H. F. Yang, B. P. Xie, F. Q. Song, P. Dudin, T. K. Kim, M. Hoesch, P. Kumar Das, I. Vobornik, X. G. Wan, and D. L. Feng, arXiv:1503.01422 [Phys. Rev. Lett. (to be published)].
[12] A. Mar, S. Jobic, and J. A. Ibers, J. Am. Chem. Soc. **114**, 8963 (1992).
[13] C. C. Homes, M. Reedyk, D. A. Crandles, and T. Timusk, Appl. Opt. **32**, 2976 (1993).
[14] M. Dressel and G. Grüner, *Electrodynamics of Solids* (Cambridge University Press, Cambridge, U.K., 2001).
[15] F. Wooten, *Optical Properties of Solids* (Academic, New York, 1972), pp. 244–250.
[16] J. W. Allen and J. C. Mikkelsen, Phys. Rev. B **15**, 2952 (1977).
[17] A. Puchkov, D. N. Basov, and T. Timusk, J. Phys.: Condens. Matter **8**, 10049 (1996).
[18] D. Wu, N. Barišić, P. Kallina, A. Faridian, B. Gorshunov, N. Drichko, L. J. Li, X. Lin, G. H. Cao, Z. A. Xu, N. L. Wang, and M. Dressel, Phys. Rev. B **81**, 100512(R) (2010).
[19] R. N. Gurzhi, Soviet Phys. JETP **8**, 673 (1959).
[20] D. L. Maslov and A. V. Chubukov, Phys. Rev. B **86**, 155137 (2012).
[21] C. Berthod, J. Mravlje, X. Deng, R. Žitko, D. van der Marel, and A. Georges, Phys. Rev. B **87**, 115109 (2013).
[22] P. L. Cai, J. Hu, L. P. He, J. Pan, X. C. Hong, Z. Zhang, J. Zhang, J. Wei, Z. Q. Mao, and S. Y. Li, Phys. Rev. Lett. **115**, 057202 (2015).
[23] D. J. Singh, *Planewaves, Pseudopotentials and the LAPW method* (Kluwer Academic, Boston, 1994).
[24] D. Singh, Phys. Rev. B **43**, 6388 (1991).
[25] P. Blaha, K. Schwarz, G. K. H. Madsen, D. Kvasnicka and J. Luitz, WIEN2k, *An Augmented Plane Wave Plus Local Orbitals Program for Calculating Crystal Properties* (Techn. Universität Wien, Austria, 2001).
[26] See Supplemental Material at http://link.aps.org/supplemental/10.1103/PhysRevB.92.161109 for details of the electronic structure calculations.
[27] C. Ambrosch-Draxl and J. O. Sofo, Comput. Phys. Commun. **175**, 1 (2006).
[28] W.-D. Kong, S.-F. Wu, P. Richard, C.-S. Lian, J.-T. Wang, C.-L. Yang, Y.-G. Shi, and H. Ding, Appl. Phys. Lett. **106**, 081906 (2015).